eprints@whiterose.ac.uk
https://eprints.whiterose.ac.uk/

A Unifying Model of Mixed Inertial Modes in the Sun

Rekha Jain[1] , Bradley W. Hindman[2,3] , and Catherine Blume[2]

[1] School of Mathematics and Statistics, University of Sheffield, S3 7RH UK; R.Jain@sheffield.ac.uk
[2] JILA, University of Colorado, Boulder, CO 80309-0440, USA
[3] Department of Applied Mathematics, University of Colorado, Boulder, CO 80309-0526, USA

Abstract

We present an analytical model that unifies many of the inertial waves that have been recently observed on the surface of the Sun, as well as many other modes that have been theoretically predicted—but have yet to be observed—into a single family of *mixed inertial modes*. By mixed, we mean that the prograde- and retrograde-propagating members of this family have different restoring forces and hence different behavior. Thermal Rossby waves exist as prograde-propagating waves, while the high-frequency retrograde (HFR) wave is one example of a member of the retrograde branch. This family of mixed modes has fully 3D motions that satisfy the anelastic form of the continuity condition. As such, the horizontal velocity is both vortical and divergent with the later flow component associated with a dynamically important radial velocity. The modes are differentiated by the number of nodes in latitude, with the lowest latitudinal order corresponding to the traditional thermal Rossby wave of Busse, the first latitudinal overtone to the mixed mode of Bekki et al., and the second overtone to the HFR wave discovered by Hanson et al. There also exist infinitely more modes of higher latitudinal order whose frequencies increase as the order increases. These higher overtones may correspond to many of the inertial modes that have been recently identified by numerical eigenmode solvers.

Unified Astronomy Thesaurus concepts: Solar convective zone (1998); Solar interior (1500); Stellar oscillations (1617); Internal waves (819); Astrophysical fluid dynamics (101); Hydrodynamics (1963)

1. Introduction

The recent detection of inertial waves on the Sun (e.g., Löptien et al. 2018) has renewed interest in such waves in the solar context, as they are perceived as a potential diagnostic of the solar interior, in particular the convection zone's super-adiabaticity (e.g., Gilman 1987; Gizon et al. 2021; Hindman & Jain 2023). The number of distinct varieties of waves has now begun to proliferate. The initial detection of sectoral equatorial Rossby waves (Löptien et al. 2018; Hanson et al. 2020) was quickly followed by critical-latitude and high-latitude inertial modes (Gizon et al. 2021), and more recently the high-frequency retrograde (HFR) waves (Hanson et al. 2022).

Recent efforts to characterize the HFR modes using numerical eigensolvers have found predominately horizontal motions at the surface and fully 3D motions in deeper layers. The existence of a significant radial velocity component distinguishes them from the highly toroidal equatorial Rossby waves (Triana et al. 2022; Bekki 2024; Bhattacharya & Hanasoge 2023). A further complication has arisen from the studies of Triana et al. (2022) and Bhattacharya & Hanasoge (2023), who report on a set of modes that are likely the $n = 1$ radial overtones of these HFR modes.

In addition to observational evidence, there are many inertial waves that have only appeared in theoretical calculations and numerical simulations. Prograde-propagating thermal Rossby waves (e.g., Roberts 1968; Busse 1970; Calkins et al. 2013; Hindman & Jain 2022) have long been predicted theoretically. Low-frequency equatorially trapped waves for incompressible fluids have been studied in the past (e.g., Bretherton 1964;

Matsuno 1966; Zhang 1993). More recently Bekki et al. (2022b) identified a "mixed inertial mode" whose dispersion relation spans both prograde and retrograde waves. When prograde, the mixed mode corresponds to the thermal Rossby wave of Roberts (Roberts 1968). When retrograde, the mode possesses horizontal velocities that are reminiscent of a Rossby wave with radial nodes. Bekki et al. (2022a, 2022b) dubbed this mode mixed because it is akin to the mixed Yanai mode (Gill 1982), which is an internal gravity wave when prograde and a Rossby wave when retrograde.

Although equatorial Rossby waves in a stably stratified atmosphere are reasonably well-understood, detailed studies of inertial waves of all sorts in an unstable stratification are still relatively sparse, and the nature of the wave cavities in the Sun's convection zone remains nebulous. Specifically, HFR modes (Hanson et al. 2022) currently lack a convincing theoretical explanation. Further, the origin of the restoring force for the retrograde branch of the mixed mode of Bekki et al. (2022a) is unclear. Presumably, there is a conservation of potential vorticity principle that can be invoked, as there are for equatorial Rossby waves and thermal Rossby waves, but the principle has yet to be uncovered. Due to the structure of the mixed mode's horizontal flow field, Bekki et al. (2022a) suggested that the mode is an equatorial Rossby wave with one radial node. However, unlike an equatorial Rossby wave, the mode appears to have significant vertical motion, and hence this classification remains a conjecture. For this reason, Blume et al. (2024) referred to the same mode that appeared in their numerical simulations simply with the phrase retrograde inertial mode. In this Letter, we propose that many of the observed modes are a generalization of "mixed modes" (Bekki et al. 2022a), all members of the same family with varying numbers of nodes in latitude.

The Letter is organized as follows. Section 2 gives a brief description of the geometry of the solution domain. Section 3 provides the governing equations and the boundary conditions. Section 4 focuses on the dispersion relation of the resulting eigenmodes, while Section 5 presents their eigenfunctions. Finally, a brief discussion and conclusions are provided in Sections 6 and 7.

2. The Cylindrical Model

In Hindman & Jain (2022), we demonstrated that gravitational stratification modifies the propagation of thermal Rossby waves in two ways. First, the increasing pressure with depth, coupled with the compressibility of the gas, provides a compressional β-effect that leads to prograde propagation. Second, the radial density stratification can naturally trap waves generating a submerged wave cavity. How such waves are trapped latitudinally is still poorly understood; however, in Jain & Hindman (2023) we showed that when the inertial wave propagates latitudinally, they can propagate in either zonal direction, retrograde or prograde. When prograde propagating, the waves are simply thermal Rossby waves with latitudinal nodes. When retrograde propagating, the waves are some other form of inertial wave. Here we demonstrate that each latitudinal overtone is actually a mixed mode. The prograde thermal Rossby waves smoothly transition to retrograde inertial waves as the azimuthal order m passes through zero.

We accomplish this by adopting the same geometry as Jain & Hindman (2023); we solve for inertial waves within a cylindrical annulus that mimics an equatorial channel in a sphere. The sphere is mapped onto the annulus by letting the cylindrical radius r equal the spherical radius and letting the cylindrical azimuth ϕ equal the spherical longitude. Finally, we map the axial coordinate of the cylinder y onto the spherical latitude Θ through the relation $y = \Theta R_\odot$. The inner cylindrical boundary is tangent to the base of the convection zone and the outer boundary to the photosphere (at a radius of $R_\odot = 696$ Mm). We adopt a depth $D = 200$ Mm for the convection zone and a height $L = R_\odot$ for the cylindrical annulus (see also Figure 4 of Jain & Hindman 2023). This *millstone*-shaped model provides natural trapping in the radial coordinate r (through the density stratification) and trapping by imposed boundary conditions in the latitudinal coordinate Θ.

Since the top and bottom cross sections of the cylindrical annulus are flat, our model lacks a topographical β-effect. However, as we mentioned previously, the density stratification within our model leads to a compressional β-effect. The compressional effect dominates the topographical effect when there are many density scale heights across the fluid layer (Glatzmaier & Gilman 1981). With just over 10 scale heights spanning the Sun's convection zone, the topographical effect should be secondary to the compressional effect.

3. Governing Equations and the Boundary Conditions

Purely for simplicity, we ignore the curvature terms that appear in the fluid equations, and the resulting equation set corresponds to those in an equatorial f-plane with boundaries in latitude and radius. Within such geometry, Jain & Hindman (2023) derived a radial wave equation and the corresponding

local dispersion relation for low-frequency inertial waves,

$$\left[\frac{\partial^2}{\partial r^2} + k_r^2(r) \right]\left(\rho_0^{-1/2} \delta P \right) = 0, \tag{1}$$

$$k_r^2(r) = \left[\frac{2\Omega k_\phi}{\omega H} + 4k_\Theta^2 \frac{\Omega^2}{\omega^2} + k_h^2 \frac{N^2}{\omega^2} \right] - k_h^2 - k_c^2, \tag{2}$$

$$k_c^2(r) = \frac{1}{4H^2}\left(1 - 2\frac{dH}{dr} \right), \tag{3}$$

where δP is the Lagrangian pressure fluctuation, $\rho_0(r)$ is the atmosphere's mass density, $k_r(r)$ is the local radial wavenumber, and $k_c(r)$ is the acoustic-cutoff wavenumber. The density scale height is denoted by H, the buoyancy frequency by N, and the rotation rate by Ω. The wavenumbers $k_\phi = m/R_\odot$ and $k_\Theta = \lambda\pi/L$ are the longitudinal and latitudinal wavenumbers, respectively, and k_h is the total horizontal wavenumber, $k_h^2 = k_\phi^2 + k_\Theta^2$. The quantities m and λ correspond to the azimuthal order and the latitudinal order of the wave mode.

In the local dispersion relation (Equation (2)), the three terms in the square brackets lead to radial propagation, with the first two producing inertial waves and the last responsible for internal gravity waves. The first of the inertial terms captures the compressional β effect and is sensitive to the direction of zonal propagation and to the density stratification. For prograde waves ($\omega/k_\phi > 0$), the term is positive and enables thermal Rossby waves. The second term in square brackets is proportional to k_Θ^2 and hence is positive only when the wave is latitudinally propagating. This term generates the traditional inertial oscillations that require variation along the rotation axis (e.g., Bryan 1889; Greenspan 1968; Rieutord & Valdettaro 2018). Such waves can be either retrograde or prograde propagating. When prograde, this term modifies the cavity for thermal Rossby waves by essentially adding an additional restoring force.

If one considers a specific atmosphere and appropriate boundary conditions in radius and latitude, Equations (1) and (2) result in global eigenmodes. Jain & Hindman (2023) considered a neutrally stable polytrope chosen to represent the Sun's convection zone. In such an atmosphere, the buoyancy frequency is identically zero, $N = 0$, and the waves present are purely inertial. The internal gravity waves are removed. We found that in such an isentropic atmosphere, the governing equation for atmospheric waves reduces to Whittaker's equation, which has analytic solutions (see Hindman & Jain 2022, 2023; Jain & Hindman 2023). For the millstone model that we are using here, the solutions can be expressed using Whittaker's function $\mathcal{M}$ (see Abramowitz & Stegun 1968),

$$\delta P(\phi, \Theta, r; t) = e^{im\phi} \cos\left[\lambda\pi\left(\frac{R_\odot}{L}\Theta + \frac{1}{2} \right) \right]$$
$$\times \mathcal{M}_{\kappa\mu}(\zeta)\, e^{-i\omega t}, \tag{4}$$

where ω is the wave's temporal frequency, ζ is a potentially complex nondimensional depth,

$$\zeta = 2k_h \sqrt{1 - \varpi^2}\, (R_\odot - r), \tag{5}$$

and the parameters κ, μ, and ϖ are defined through the relations

$$\kappa \equiv \frac{\alpha\Omega}{\omega}\frac{k_\phi/k_h}{\sqrt{1-\varpi^2}}, \quad \mu \equiv \frac{\alpha+1}{2}, \quad \varpi^2 \equiv \frac{4\Omega^2}{\omega^2}\frac{k_\Theta^2}{k_h^2}. \quad (6)$$

The parameter α is the polytropic index, which for a neutrally stable atmosphere depends explicitly on γ, the gas's adiabatic exponent, $\alpha = (\gamma - 1)^{-1}$.

This solution (Equation (4)) has been constructed such that it satisfies both radial and latitudinal boundary conditions. The solution is regular at the photosphere, where $r = R_\odot$ (and $\zeta = 0$). Further, the solution satisfies Neumann boundary conditions in latitude,

$$\frac{\partial \delta P}{\partial \Theta}(\Theta = \pm L/2R_\odot) = 0. \quad (7)$$

With such a boundary condition, the latitudinal order takes on nonnegative integer values, $\lambda \in [0, 1, 2, 3,...]$. In order to satisfy an appropriate boundary condition on the inner cylinder, one must choose the eigenvalue κ correctly. Through Equation (6), this is equivalent to choosing eigenfrequencies. We opt to apply a Dirichlet boundary condition at the base of the convection zone, $\delta P(r = R_\odot - D) = 0$. There are an infinite number of radial overtones each with a different eigenfrequency ω_n labeled by the radial order n, which indicates the number of radial nodes in the eigenfunction for the Lagrangian pressure fluctuation. Here, we will only explicitly consider the radial fundamental $n = 0$ and the first radial overtone $n = 1$.

The components of the velocity can be derived from the Lagrangian pressure fluctuation through differential operators. In the low-frequency limit, where the waves have frequencies that are much smaller than those of surface gravity waves (i.e., $\omega^2 \ll gk_\phi$ and $\omega^2 \ll gk_\Theta$), the differential operators reduce to the following relationships:

$$u_\phi = -\frac{\omega}{g\rho_0 k_h^2}\left(k_\phi\frac{\partial \delta P}{\partial r} - \frac{2\Omega}{\omega}k_\Theta^2 \delta P\right), \quad (8)$$

$$u_\Theta = \frac{i\omega}{g\rho_0 k_h^2}\frac{1}{R_\odot}\frac{\partial}{\partial \Theta}\left(\frac{\partial \delta P}{\partial r} + \frac{2\Omega}{\omega}k_\phi \delta P\right), \quad (9)$$

$$u_r = \frac{i\omega}{g\rho_0}\delta P, \quad (10)$$

where g is the gravitational acceleration and u_ϕ, u_Θ, and u_r are the three velocity components in the longitudinal, latitudinal, and radial directions, respectively.

4. Dispersion Relation

It is clear from Equation (4) that the eigenfunctions consist of a family of modes with varying numbers of nodes in latitude. Figure 1 shows the eigenfrequencies as a function of azimuthal order m for the five lowest latitudinal orders. For clarity of presentation, only the radial fundamental modes ($n = 0$) and the first overtone ($n = 1$) are illustrated. For reference, we also mark the frequencies of equatorial Rossby waves with the gray filled circles, using the theoretical dispersion relation $\omega = -2m\Omega/k_h^2R_\odot^2$. Further, we have included the zero-frequency geostrophic mode (horizontal gray line) that resides within a neutrally stable atmosphere (see Hindman & Jain 2022). Prograde waves are in the first and third quadrants
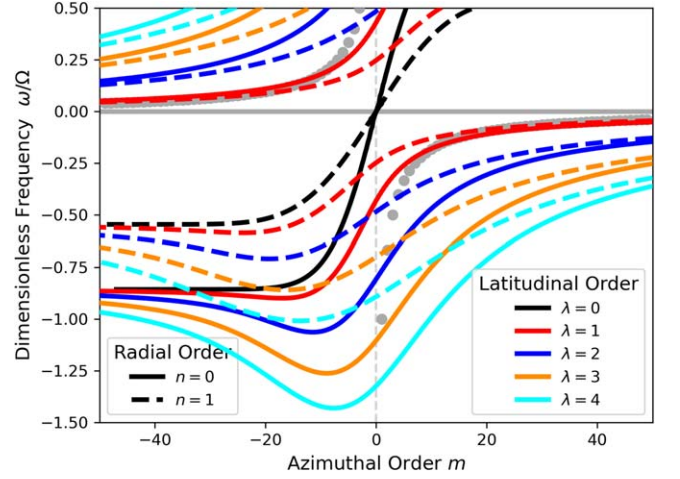

Figure 1. Eigenfrequencies of inertial modes trapped radially and latitudinally within a millstone-shaped equatorial channel. The dimensionless eigenfrequencies are plotted as a function of the azimuthal order, m. Different colors correspond to different latitudinal orders, λ, as indicated in the legend. The solid and dashed curves are for radial orders $n = 0$ and 1, respectively. The horizontal gray line corresponds to the zero-frequency geostrophic mode. For reference, we also show the frequencies of equatorial Rossby waves with the gray filled circles, given by $\omega/\Omega = -2m/k_h^2R_\odot^2$. The modes with positive zonal phase speed, $\omega/m > 0$, propagate in the prograde direction, whereas modes with negative phase speed $\omega/m < 0$ are retrograde propagating.

where $\omega/m > 0$. Retrograde waves correspond to those in the second and fourth quadrants where $\omega/m < 0$. As such, the dispersion diagram has reflection symmetry across the origin.

All of the modes that possess at least one node in latitude are mixed, in the sense that the dispersion relation for a given latitudinal order consists of both prograde and retrograde solutions that smoothly join each other as m passes through zero. The prograde branch has a wave cavity arising from the first term in square brackets in Equation (2). The retrograde branch has a different cavity produced by the second term in the square brackets. The fundamental latitude mode ($\lambda = 0$) lacks this property, as it lacks retrograde solutions. For $\lambda = 0$, only the prograde branch exists, and it corresponds to the thermal Rossby wave of Busse (Busse 1970).

5. Eigenfunctions

Using Equations (8)–(10), one can easily deduce that the motions are anelastic,

$$\nabla \cdot (\rho_0 u) = 0, \quad (11)$$

instead of incompressible ($\nabla \cdot u = 0$). Specifically, the horizontal motions, Equations (8) and (9), consist of both a vortical piece and a divergent piece. This is readily apparent in Figure 2, which presents the horizontal flow field for three distinct retrograde propagating eigenmodes, all with $m = 2$ and $n = 0$, and with λ ranging from 1 to 3. The color image underlying the vector field shows the radial vorticity ξ_r of the corresponding mode, which can be shown to be directly proportional to the latitudinal derivative of the Lagrangian pressure fluctuation,

$$\xi_r = \frac{1}{R_\odot}\left(\frac{\partial u_\Theta}{\partial \phi} - \frac{\partial u_\phi}{\partial \Theta}\right) = -\frac{2\Omega}{g\rho_0 R_\odot}\frac{\partial \delta P}{\partial \Theta}. \quad (12)$$
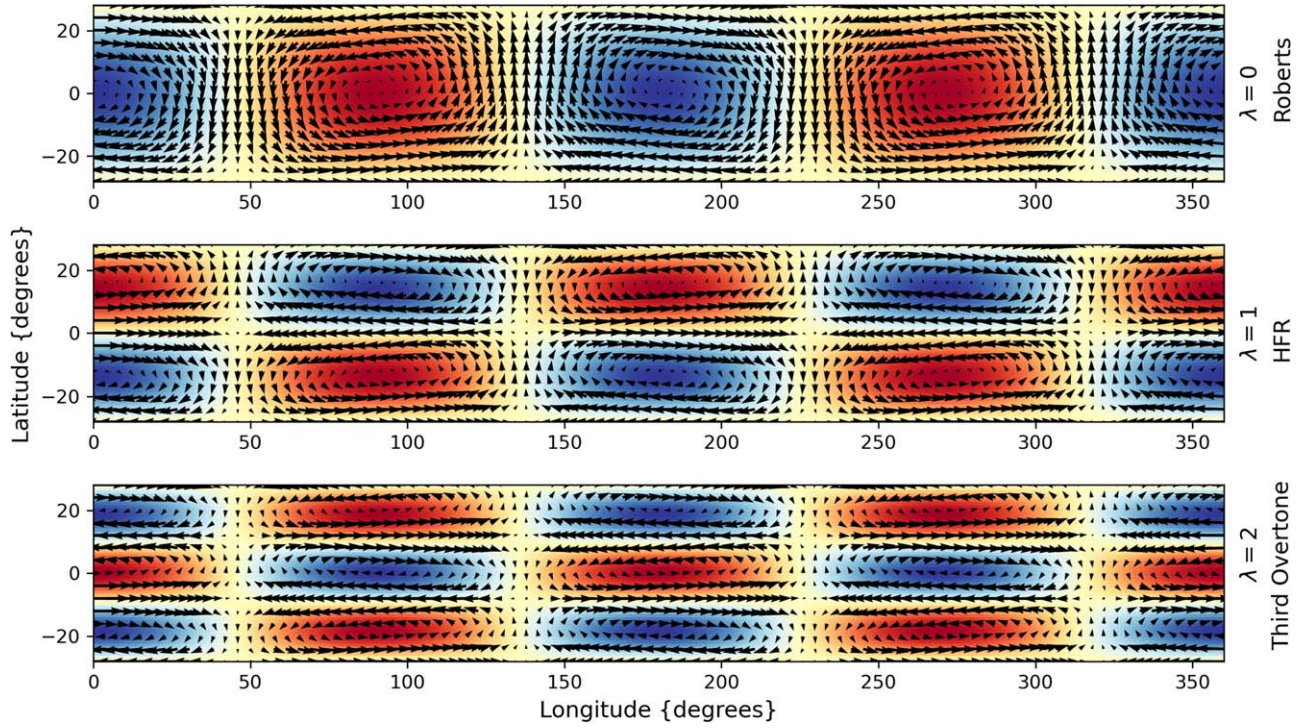
Figure 2. Arrows indicate the horizontal flow for three distinct modes as a function of longitude and latitude for a depth that is 2 Mm below the photosphere. The underlying color image shows the radial vorticity component with red tones for positive vorticity and blue tones for negative. Each panel illustrates the mode with azimuthal order $m = 2$ but for different latitudinal orders, as indicated to the right. All flow fields are clearly both vortical and horizontally divergent.

We have chosen not to illustrate the fundamental latitudinal mode, $\lambda = 0$, because its eigenfunction is a constant function of latitude, and the latitudinal velocity component and the radial vorticity are identically zero everywhere.

Figure 3 presents the radial eigenfunctions for the zonal velocity u_ϕ, the radial vorticity ξ_r, and the horizontal divergence Δ_h. This latter quantity is directly proportional to the radial derivative of the Lagrangian pressure fluctuation,

$$\Delta_h = \frac{1}{R_\odot}\left(\frac{\partial u_\phi}{\partial \phi} + \frac{\partial u_\Theta}{\partial \Theta} \right) = -\frac{i\omega}{g\rho_0}\frac{\partial \delta P}{\partial r}. \quad (13)$$

Figures 2 and 3 clearly demonstrate that the radial vorticity and the horizontal divergence have similar magnitudes. Further, as expected, the number of nodes that appear in the eigenfunction in latitude and radius is variable-dependent. For example, The fundamental radial mode ($n = 0$) has zero nodes in latitude in the radial vorticity ξ_r, the radial velocity u_r, and the Lagrangian pressure fluctuation δP. Whereas, the two horizontal velocity components, u_ϕ and u_Θ, and the horizontal divergence Δ_h each have one radial node. Similarly, the first latitudinal overtone ($\lambda = 1$) has one latitudinal node in the eigenfunctions for the zonal velocity, radial velocity, horizontal divergence, and Lagrangian pressure fluctuation, and zero latitudinal nodes in the latitudinal velocity and the radial vorticity.

6. Discussion

6.1. A Unified Family of Mixed Modes

The central premise of this work is that the family of mixed modes that we have identified encompasses a wide variety of inertial waves that have been previously observed or theoretically predicted. Our supposition is based on the
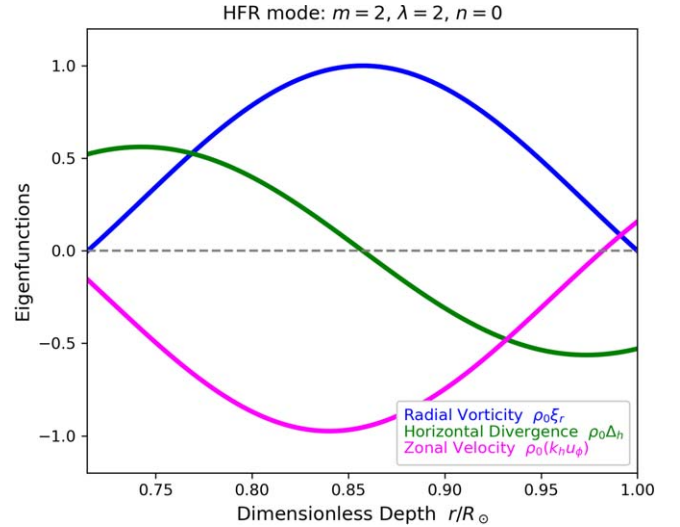

Figure 3. Radial eigenfunctions for an HFR mode ($\lambda = 2$) for an azimuthal order $m = 2$ and for the radial fundamental $n = 0$. The eigenfunctions are shown as a function of dimensionless radius, $r/R_\odot$. The real part of the zonal velocity (magenta curve) and radial vorticity (blue) are illustrated, whereas the imaginary part of the horizontal divergence (green curve) is shown. Each eigenfunction is scaled by the mass density ρ_0 and the zonal velocity is further scaled by the horizontal wavenumber k_h so that it has the same units as the other variables. The radial vorticity and horizontal divergence have similar magnitudes but differing radial structures.

similarity in the eigenfrequencies, how those frequencies vary with the azimuthal order m, the direction of propagation (prograde versus retrograde), and the equatorial symmetry of the eigenfunctions.

To illustrate our proposed unifying model, we provide a summary in Figure 4. This figure provides a close-up view of the dispersion relation for the radial fundamental $n = 0$ for
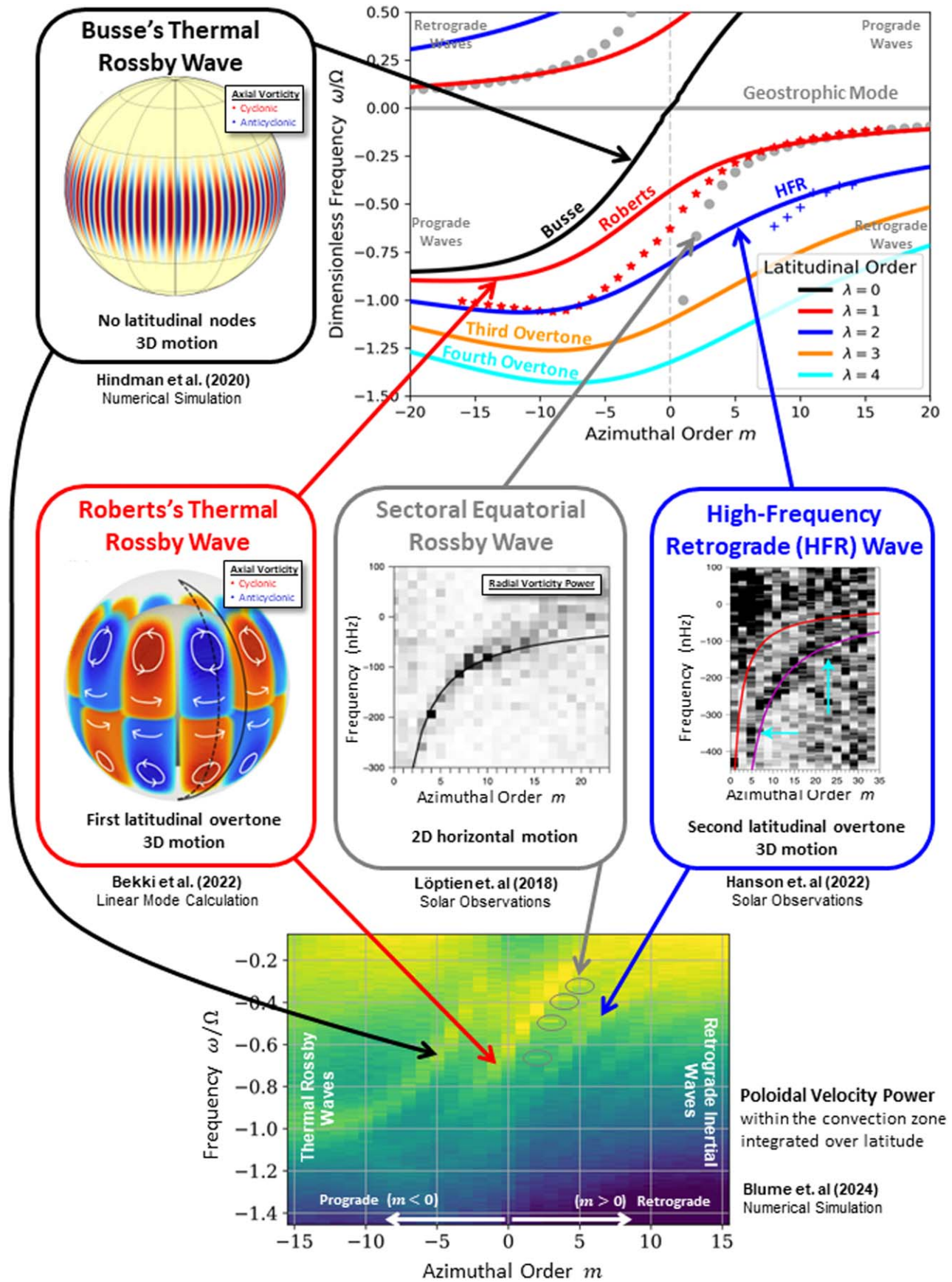
Figure 4. Summary of the family of mixed inertial waves that we explore here and their identification with inertial waves as reported in a selection of previous studies. We argue that many of the waves previously discovered through observations or through theoretical calculations, including the HFR mode, are simply latitudinal overtones within the same family of mixed inertial modes. We have overplotted the observed frequencies of HFR modes (Hanson et al. 2022) with blue pluses and the "mixed modes" of Bekki et al. (2022a) with red asterisks.

various latitudinal overtones. In addition, we present several of the previously identified inertial waves; we have overplotted the observed frequencies of HFR modes (Hanson et al. 2022) with blue pluses and the "mixed modes" of Bekki et al. (2022a) with red asterisks.

Specifically, we propose that all prograde-propagating waves are thermal Rossby waves. The lowest latitudinal order $\lambda = 0$ corresponds to the traditional thermal Rossby wave of Busse (Busse 1970; Calkins et al. 2013; Hindman et al. 2020; Hindman & Jain 2022) and the first latitudinal overtone ($\lambda = 1$) to the thermal Rossby wave of Roberts (Roberts 1968; Bekki et al. 2022a). Note that such waves do not require an unstable stratification. The restoring force is purely the Coriolis force and, in an unstable atmosphere, buoyancy only leads to instability for short wavelength waves. The wavenumber, which marks the transition from stable to unstable, depends on the buoyancy frequency (see Hindman & Jain 2023). In the limit of neutral stability, this transition wavenumber becomes infinitely large and all wavelengths become stable.

On the retrograde side of the diagram, the first latitudinal overtone ($\lambda = 1$) corresponds to the mixed mode identified by Bekki et al. (2022a), the second overtone ($\lambda = 2$) to the HFR wave discovered by Hanson et al. (2022), and the third overtone ($\lambda = 3$) seems to correspond to the high-frequency, equatorially symmetric mode reported in Bhattacharya & Hanasoge (2023). Finally, we note that the frequency dependence for our $\lambda = 2$, $n = 1$ overtone (see Figure 1) has similar behavior to the radial overtone noted in eigenmode calculations by Triana et al. (2022) and Bhattacharya & Hanasoge (2023). It is interesting to note that this entire family of mixed modes is also present in 3D dynamo simulations of the Sun's convection zone and radiative interior (Blume et al. 2024).

Note that the comparison in Figure 4 between our analytically derived frequencies and those from observations and numerical eigensolvers is qualitative as our assumption of an f-plane geometry at the equator does not take into account the curvature effects, which produce natural equatorial trapping of the waves. Further, it is likely that the spatial extent of the latitudinal cavity depends on the azimuthal order m, which our simple model ignores. For example, the latitudinal turning point for equatorial Rossby waves (which have spherical harmonic eigenfunctions) depends on the ratio m/l, where l is the harmonic degree. Finally, the inertial modes are all very sensitive to the superadiabaticity of the convection zone, with the relevant parameter being the ratio of the buoyancy frequency to the rotation rate, $|N|/\Omega$. For tractability, we have adopted neutral stability; but, in reality, the upper portion of the convection zone has a superadiabaticity that is probably important, $|N| > \Omega$.

6.2. Truly 3D Fluid Motions

Unlike equatorial Rossby waves, the modes that we explore here have a significant radial component of the velocity. This can be seen directly in Equations (8)–(10) where modes with frequencies ω close to the rotation rate Ω, clearly have a radial velocity comparable in magnitude to the horizontal components. The relative importance of the radial velocity can also be seen indirectly in Figures 2 and 3. Using the anelastic relation, we recognize that the existence of the horizontal divergence

arises from a significant radial velocity component,

$$\Delta_h = -\frac{\partial(\rho_0 u_r)}{\partial r}. \tag{14}$$

The fact that the horizontal velocity field is both vortical and divergent requires that the radial velocity is dynamically significant.

7. Conclusion

Using a simple analytical model of a neutrally stable polytrope in an equatorial f-plane geometry, we demonstrate the existence of a family of mixed inertial modes. The prograde-propagating branch corresponds to thermal Rossby waves and the retrograde-propagating branch includes many waves that have been identified previously in the literature. We suggest that many of the inertial waves that have been either observed or found with numerical eigenmode solvers, including the HFR mode, are in fact all related, being latitudinal overtones mixed with the prograde thermal Rossby waves. In summary, on the basis of our model, we reckon that there are only two unique families of propagating inertial waves in the solar convection zone: the equatorial Rossby waves, which are primarily horizontal in motion, and a spectrum of mixed modes that possess truly 3D motions.

ORCID iDs

Rekha Jain ⓘ https://orcid.org/0000-0002-0080-5445
Bradley W. Hindman ⓘ https://orcid.org/0000-0001-7612-6628
Catherine Blume ⓘ https://orcid.org/0000-0001-9004-5963

References

Abramowitz, M., & Stegun, I. A. 1968, Handbook of Mathematical Functions with Formulas, Graphs and Mathematical Tables (New York: Dover)
Bekki, Y. 2024, A&A, 682, A39
Bekki, Y., Cameron, R. H., & Gizon, L. 2022a, A&A, 662, A16
Bekki, Y., Cameron, R. H., & Gizon, L. 2022b, A&A, 666, A135
Bhattacharya, J., & Hanasoge, S. M. 2023, ApJS, 264, 21
Blume, C. C., Hindman, B. W., & Matalsky, L. I. 2024, ApJ, in press
Bretherton, F. P. 1964, Tell, 16, 181
Bryan, G. H. 1889, RSPTA, 180, 187
Busse, F. H. 1970, JFM, 44, 441
Calkins, M. A., Julien, K., & Marti, P. 2013, JFM, 732, 214
Gill, A. 1982, Atmosphere—Ocean Dynamics, International Geophysics Series, Vol. 30, (San Diego, CA: Academic Press)
Gilman, P. A. 1987, ApJ, 318, 904
Gizon, L., Cameron, R. H., Bekki, Y., et al. 2021, A&A, 652, L6
Glatzmaier, G. A., & Gilman, P. A. 1981, ApJS, 47, 103
Greenspan, H. 1968, The Theory of Rotating Fluids (London: Cambridge Univ. Press)
Hanson, C. S., Gizon, L., & Liang, Z.-C. 2020, A&A, 635, A109
Hanson, C. S., Hanasoge, S., & Sreenivasan, K. R. 2022, NatAs, 6, 708
Hindman, B. W., Featherstone, N. A., & Julien, K. 2020, ApJ, 898, 120
Hindman, B. W., & Jain, R. 2022, ApJ, 932, 68

Hindman, B. W., & Jain, R. 2023, ApJ, 943, 127
Jain, R., & Hindman, B. W. 2023, ApJ, 958, 48
Löptien, B., Gizon, L., Birch, A. C., et al. 2018, NatAs, 2, 568
Matsuno, T. 1966, JMeSJ, 44, 25

Rieutord, M., & Valdettaro, L. 2018, JFM, 844, 597
Roberts, P. H. 1968, RSPTA, 263, 93
Triana, S. A., Guerrero, G., Barik, A., & Rekier, J. 2022, ApJL, 934, L4
Zhang, K. 1993, JFM, 248, 203